**MSc in Photonics**

Universitat Politècnica de Catalunya (UPC)
Universitat Autònoma de Barcelona (UAB)
Universitat de Barcelona (UB)
Institut de Ciències Fotòniques (ICFO)

PHOTONICS**BCN**

http://www.photonicsbcn.eu

*Master in Photonics*

## MASTER THESIS WORK

# Study of SiPM segmentation in ToF-PET from the optical perspective

**Antonio Mariscal Catstilla**

**Supervised by Prof. Bruno Julià Díaz , (UB)**

**Supervised by Dr. Sergio Gomez, (ICCUB)**

**Supervised by Dr. David Sanchez, (ICCUB)**

Presented on date 9th September 2021

Registered at

Escola Tècnica Superior d'Enginyeria de Telecomunicació de Barcelona

# Study of SiPM segmentation in ToF-PET from the optical perspective

**Antonio Mariscal Castilla**

Institut de Ciències del Cosmos (ICCUB), Technologica Unit, Carrer de Martí i Franquès, 1, planta 3, 08028 Barcelona.

E-mail: antonio.mariscal@estudiantat.upc.edu

September 2021

**Abstract.** Introduction of SiPM sensor in positron emission tomography (PET) technique has allowed the use of time-of-flight (ToF) information, which improves the imaging technique performance. However, there is still a lot of room for improvement. One approach to increase the image resolution, consists on segmenting the SiPM area into smaller areas and apply an algorithm to recover the maximum possible information. In the literature, it has been shown that this approach can increase the coincidence time resolution (CTR). Here, we study how segmenting the sensor area into smaller sensors affects the time resolution from an optical perspective. In order to accomplish this, we simulated different segmentations and studied how the segmentation affects the CTR of the system. Results show that the CTR doesn't degrade significantly when segmenting the sensor in a few channels. Therefore, it can be expected an increase on the total CTR if a increase on the electronics performance can be achieved.

**Keywords**: silicon photomultiplier, scintillator crystal, simulation, positron emmission tomography, tof-pet

## 1. Introduction

In the last decades, developments on semiconductor technology has made the Silicon Photomultipliers (SiPM) sensor an excellent choice due to its great timing response and capacity to single-photon detection. Consequently, it has been used in a wide range of applications, finding a great success in medical imaging [1]. Concretely, SiPM sensor has been used to improve the performance of Time-of-Flight Positron Emission Tomography (TOF-PET) [2] .

Positron Emission Tomography (PET) [3] is an image technique that consist on the administration to a patient of a biomolecule labeled with a radioactive isotope which disintegrates via a $\beta^+$-decay, resulting in the emission of a positron that is annihilated with an electron inside the organ under study. As a result of this reaction, two almost back-to-back travelling 511 keV gamma-rays are emitted. Posteriorly, the two photons are detected almost simultaneously using a ring detector. The line formed by the detection of the two photons is called line-of-response (LOR). The location within the LOR is given by the time difference between the detection times of the two photons, called time-of-flight (TOF) difference. Depending if the apparatus make use of the ToF difference or not, we call the imaging technique, ToF-PET or PET. In this work we are

going to focus on ToF-PET, whose main factor affecting imaging performance is system coincidence time resolution (CTR) [2].

The basic PET module [4] is formed by a scintillator crystal that convert the gamma photon into visible light, a photo-sensor which convert the optical photons in carriers and dedicated electronics that reads the signal generated by the sensor and converts it in readable data that later will be used to reconstruct the image of the patient. Thus, the contribution to the time jitter (or the CTR when considering two detectors in coincidence) can be separated in three main parts: scintillator crystal, SiPM and electronics (fig. 1a) . In the case of the scintillator crystal, three phenomena contribute to the time jitter: the fluctuation of the depth of interaction (DOI) of the gamma photon ($t_{depth}$), the scintillator process that determines the emission time of every optical photon ($t_{scint.}$) and the needed time for the optical photon to arrive at the photo-sensor, called Transient Time Spread ($t_{TTS}$), which depends on the traveled path. For the photo-sensor, the main factors are the avalanche process inside the solid state detector and the Photo-Detection Efficiency (PDE). Since the avalanche process is a stochastic process, the detection time depends on the gamma event translating this into a time jitter at the single photon level ($t_{SPTR}$). Finally, the electronics that read the analog signal is processed by a Front-End (FE), which converts the electrical signal generated by the SiPM to an analog signal containing the time arrival of the photons (ToA) electronics and the energy response (i.e., the amount of photons detected) in order to identify the 511 KeV events. Moreover, the electronics employs a Time to Digital Converter (TDC) or an analog to Digital Converter (ADC) Time to Digital Converter (TDC), which digitizes the ToA information and converts it to a digital format that can be processed by the data acquisition system. These devices introduce fluctuations on the ToA due to electronic noise, which in turns introduces a time jitter that is represented by $t_{elec.}$.

In [4], David Sanchez et al. found that segmenting the area of a SiPM sensor into $m$ smaller areas, reading them with independent channels in an ASIC and internally summing them to recover the full signal, improved the time resolution by 20% in the case of segmenting a single sensor of 3 $mm$ $x$ 3 $mm$ into 4 sensors of 1.5 $mm$ $x$ 1.5 $mm$ (fig. 1b). Motivated by this result, the objective of this work is to study how different segmentation set-ups affects the time resolution (CTR) from the optical standpoint, i.e, considering only the SiPM, the optical coupling and the Scintillator Crystal. In order to accomplish this, we have compared an ideal digital SiPM with an analog one [5]. The main difference between them is that in the analog SiPM, all Single-Photon Avalanche Diodes (SPAD) are connected in parallel to a single readout electronics (FE and TDC), whereas in the digital SiPM, every SPAD is connected to its own readout electronics [5]. Therefore, a digital SiPM gives access to all photons detected in one gamma event while a analog SiPM provides only a single signal representing the arrival time of all of the photons, i.e., the summation of all events.

In the next sections, we will give an explanation of the software used to simulate the system and process all the data. The most significant results and a discussion about them will be presented. Finally, future lines of work will be outlined.

## 2. Methodology

### *2.1. Gate*

GATE [6] is an advanced open-source software [6] devoted to numerical simulations in medical imaging and radiotherapy, whose simulation engine is the GEANT4 [7]. In

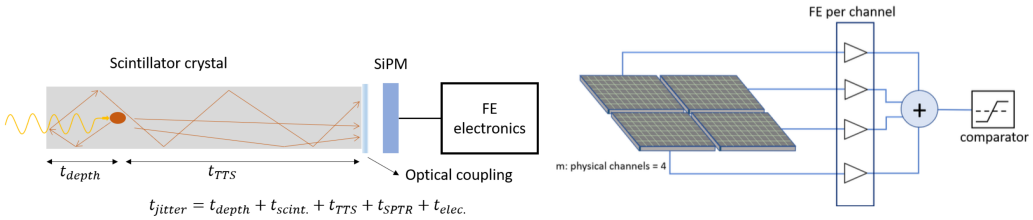


(a) Contributions to the time jitter in the PET detector from crystal, SiPM and electronics.

(b) SiPM sensor segmented in 4 channel and its analog summation scheme. Each channel corresponds to a square geometric subarea in which the sensor is divided.

Figure 1: Scheme representation of the contribution to the time jitter (1a) and the segmentation of a sensor (1b) [4].

order to run a simulation in GATE, first, a CTR setup (fig. 2) has to be defined. This setup is compromised of a nuclear radioactive $^{22}$Na point source located between two scintillator crystals of adjustable length, being both covered by teflon (to maximize the light collection) by default and whose interface surfaces can be defined using the DAVIS model [8], which allows to generate our own parameters by calculating the reflectance properties from the crystal topography previously measured with an atomic force microscope or a confocal laser scanning microscope. Then, the scintillator crystals are coupled to a sensor through a layer of optical grease, whose optical properties can be adjusted, and the sensor PDE spectrum, which usually is proportionated by the manufacturer, can be introduced as a parameter as well.

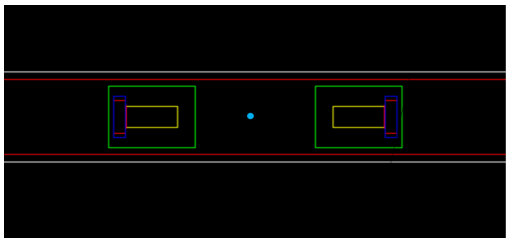

Figure 2: Image from GATE of the CTR setup, where it can be seen the $^{22}$Na source (Cyan), the detector module (green) and inside, the scintillator (yellow), the SiPM detector (blue) and the optical grease (red) [4].

The simulation starts with the emission of a positron from the $^{22}$Na source which annihilates with an electron and emits two back-to-back 511 keV gamma photons. Then, these photons interact with the scintillator crystal through Compton scattering or Photoelectric effect, resulting in the generation of a number of optical photons. The number of photons generated depends on the light yield of the crystals. Ultimately, a fraction of those photons arrive at the sensor at a time that depends on the traveled path through the crystal. As an output of the simulation we obtain a root file that contains the arrival times of every photon produced in the scintillator, the impact position on the sensor surface, the type of particle and the type of process by which the particle was generated.

### *2.2. PyPro*

PyPro is a python package that has been built to analyse the data outputted by GATE. It simulates digital and analogical SiPMs allowing us to change the segmentation. Additionally, it implements a method used in [4], in which the final timestamp is the average of the ToA of the photons acquired from different channels. Therefore, the number of channels averaged to obtain the final timestamp is also a parameter which can be modified. The software has several functions that allow us to calculate the CTR with respect to different segmentations, being the core functions the following ones:

- `Data Read into Channels (DRC)`:
  this function takes as an input the data from GATE, the SiPM size, the number of channels of the SiPM, the number of cells (SPADs) for every channel and the intrinsic time jitter $t_{SPTR}$ of the SiPM. It returns a data structure where each photon detected by the SiPM is saved as a function of the channel, its corresponding detector, and the event in which it was produced. Thus, for each different channel, detector and event, we have a list of photons. This list is ordered in ascending order for each channel. For example, for an event E, a detector D and a channel C we have a list of N photons $T(E, D, C)_N = \{t_1, t_2, t_3, ..., t_N\}$ where $t_1 < t_2 < t_3 < ... < t_N$, with N being the total number of photons in the channel. A time filter is introduced to discard all photons with a ToA greater than the time window of interest, since they do not affect to the CTR and therefore the data to be processed is vastly reduced. After that, the intrinsic time jitter to the photo-sensor is introduced by summing a random timestamp generated by a Gaussian distribution. The final timestamp saved for each photon is the sum of the ToA and the $t_{SPTR}$, $timestamp_{final} = t_{arrival} + t_{SPTR}$.
- `Digital Time Differences (DTD)`:
  It has as inputs the data structure returned by the DRC function, the total number of channels in the sensor , the position of the photon and the numbers of channel that we want to use for the averaging . This function returns the time differences between different detectors and events for a specific segmentation of the sensor and desired number of channels averaged.
  Suppose that a collection of photons produced in an event E have arrived at detector D, the function DRC will provide a list of photons in ascending order for each channel of sensor. The DTD function will read the data structure outputted by DRC and save the ToA of the $n_{th}$ photon of every channel in a list $T_{n_{th}}(E, D) = \{t^1_{n_{th}}, t^2_{n_{th}}, .., t^N_{n_{th}}\}$, where N is the total number of channels. This list will be ordered in ascending order, i.e., $t^1_{n_{th}} < t^2_{n_{th}} < ... < t^N_{n_{th}}$. Then, the resulting timestamp will be the average between the desired number of channels. So, in the case that the sensor is segmented into 4 channels and we want to use 2 channels to compute the average, this two channels will be the two fastest ones, i.e., $t^1_{n_{th}}, t^2_{n_{th2}}$. Posteriorly, this timestamp will be saved in a non-ordered list containing the timestamp of every event that has reached the detector. As a result, there will be two lists $T^1_D, T^2_D$, one for each detector. Finally, it will be computed the difference between each element of $T^1_D$ with each element of $T^2_D$ and it will be saved in a list.
  A representation of this list as an histogram can be seen in Fig. 3..Therefore, with this function we have access to the timestamps of all the photons that reach the sensor, providing the same information as a digital SiPM that records the timestamps of all incoming photons.

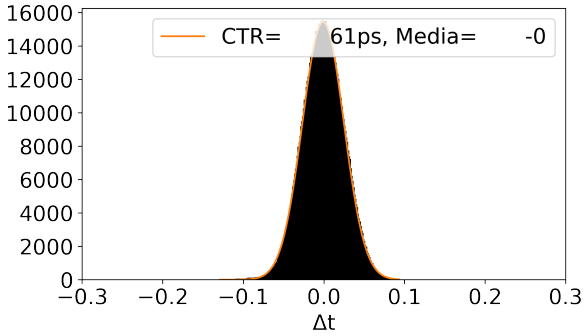


Figure 3: Histogram of the time differences for a 3 mm x 3 mm x 5 mm LSO crystal scintillator and 4-channel SiPM sensor, using the ToA of the fastest photon acquired by each channel as the timestamp.

- `Analog Time Differences (ATD)`:
  the purpose of this function is the same as the DTD function, but in this case instead of using the nth photon of each detector to compute the final timestamp, we have created a function (`SiPM Signal Generation (SSG)`) that simulates the stacking of the photons produced in a analogical SiPM for every channel in the sensor and generate the timestamp. The SSG function works as follows: first, every incoming photon is emulated as an electronic signal representing the response of the sensor connected to an electronic readout circuit. This reference signal is obtained using an electrical simulator [9] by simulating a single-channel SiPM electronic model [10] directly connected to a 20 Ω impedance, which represents the input impedance of an electronic FE (fig. 4a). Posteriorly, the SiPM signal corresponding to each photon is summed after applying a shift in the time axis corresponding to the timestamp associated to each event (stacked signal in fig. 4b and fig. 4c) . After the summation, an ideal leading edge comparator is used to generate the resulting timestamp. In fig. 4c, we can see an example of the the sum of two photons. It is worth to note that with the `SSG`, we can control the number of photons affecting to the final timestamp generated by adjusting the discriminator threshold of the ideal leading edge comparator. This method enables us to estimate the number of photons involved in the measurement.
  As the `DPD` function does, `APD` returns the time differences between different detectors and events for a specific segmentation, but instead of using the ToA of the photon as the timestamp, uses the timestamp generated by the aforementioned function `SSG`. Furthermore, it returns the mean and standard deviation of the number of photons that have contributed to the ToA for each channel.
- `CTR`:
  this function calculates the CTR from one of the previous two functions by calculating the Full Half Width Maximum (FHWM) of the timestamp histogram (fig 3). More specifically, we perform a gaussian fit of the time difference histogram obtained by the function `ATD` or `DTD` and then we calculate the standard deviation of the fitted histogram to compute the FWHM as 2.35 times the standard deviation. This can be seen in fig. 3.

The work flow consists on using the `DRC` to read the data, then using either `DTD`, if we want to simulate a digital SiPM, or `ATD`, if we want to simulate an analogic one, and then introduce the output of any of them in the `CTR` function to obtain the CTR.

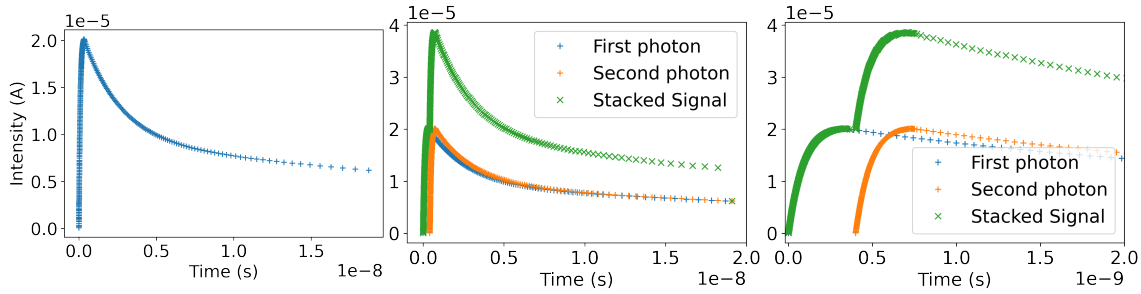


(a) Signal generated by Cadence.

(b) Signal stacked for two incoming photons.

(c) Zoom of the stacked signal.

Figure 4: Graphic representation of the operation that `SSG` does for two photons with timestamps of 1 ns and 1.5 ns.

## 3. Results

Different setups with several SiPM segmentations and scintillator lengths were studied. Regarding the scintillator, we used the inorganic Lutetium Oxyorthosilicate (LSO) crystal with two different sizes, 3 *mm* x 3 *mm* x 5 *mm*, which is the typical one used in research devices, and 3 *mm* x 3 *mm* x 20 *mm*, which is the most used in commercial machines. In the case of the SiPM segmentation, we studied sensors with 4, 9, 16, 25 and 36 channels, but this study can be extended to other segmentations. In each case, we computed the CTR for all possible number of averaged channels by simulating first the CTR setup in GATE and then using the PyPro package to compute the CTR as a function of the number of channels, the number of averaged channels and the position in the ordered list of the ToA for each channel. We also made this computation for both SiPMs, digital and analog. In case of a digital SiPM, we computed the CTR for the first, second and third photons. For the analog case, we set different discriminator thresholds representing an equivalent input signal of one (10 uA), two (30 uA) and three photons (50 uA). It is worth to note, that since the ordering of the ToA of the photons in each channel and the ordering of the channels in each detector is made in increased order, the first averaged channels are the ones with the fastest photons.

For every segmentation of the digital SiPM, we found that using the first photon to obtain a timestamp for each channel and then perform the averaging provides the best CTR (fig. 5). Additionally, we can see in fig. 5 that the CTR increases with the number of averaged channels, which doesn't happen for the cases where the second and third photon were chosen (fig. 5 and 6). Instead, in these cases, the CTR decreases as the number of averaged channels increases, until it arrives at its minimum, where it increases again until it reaches its maximum. Further, the minimum shifts towards the right when we use subsequent photons to the first. This behaviour seems to indicate that for the second and third photon the time information is more scattered, which can be recovered up to a certain point by averaging the ToA. Considering this, as we increase the order of the photon, we need to average more channels to be able to recover as maximum information as possible, which makes sense with the latter argument, since the time information will be more spread. Furthermore, we can see in fig. 5 that the information recovered for the 5 *mm* crystal for a 16 channels sensor using the third photon is bigger than for the 20 *mm* in the same conditions, being an 26% of improvement respect to the first averaged channel for the 5 *mm* versus an 6% for the 20 *mm* crystal. Therefore,

following our reasoning, in the 20 *mm* crystal the time information is more spread, which is in accordance with the literature [11].

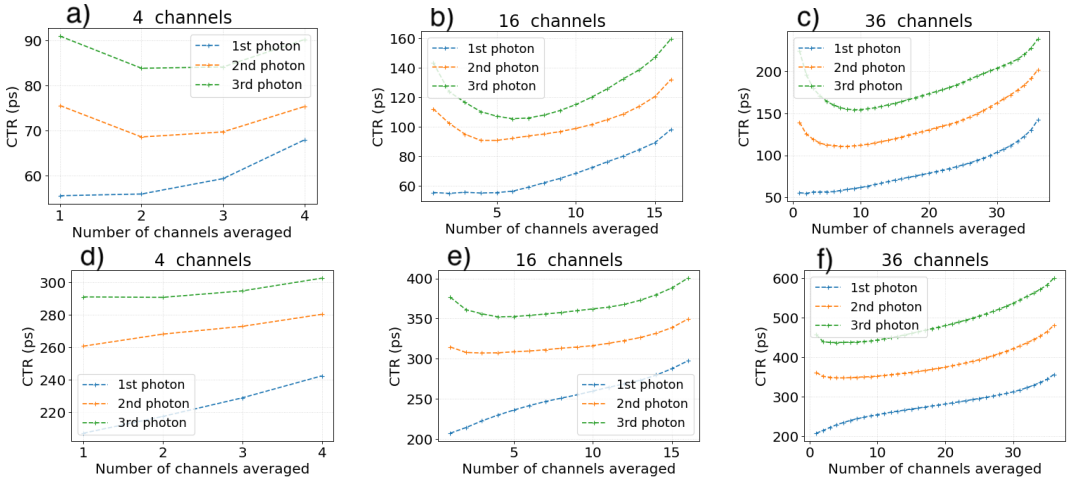


Figure 5: CTR obtained with a Digital SiPM for 5 *mm*, [a),b), c)] and 20 *mm* [d), e),f)] using different segmentations.

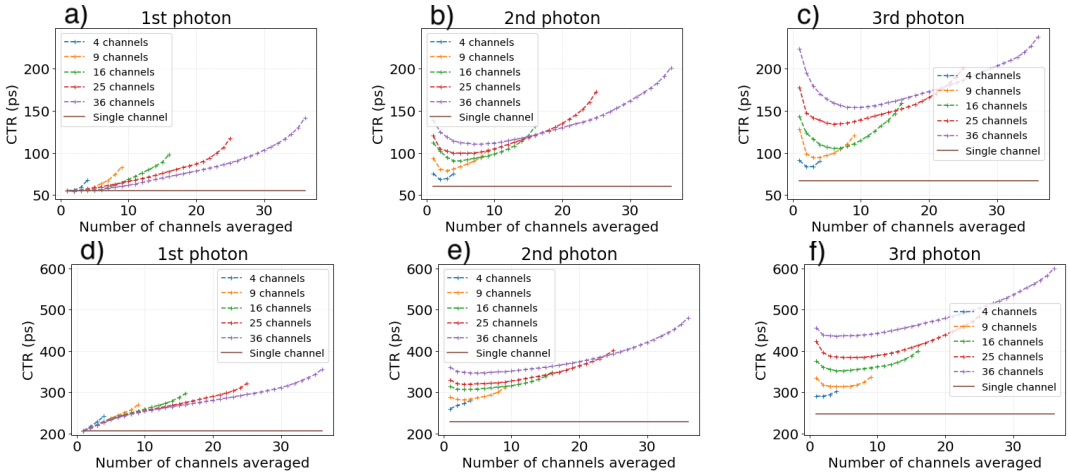


Figure 6: CTR obtained with a digital SiPM for first, second and third photon for a 5 *mm*, [a),b), c)] and a 20 *mm* [d),e), f)] LSO crystal

In fig. 6, it can be appreciated, for the second and third photon, that the CTR experience an increment as the number of averaged channels increase. A shift toward the right of the minimum CTR can be also seen. This seems to indicate that for slower photons than the fastest, segmenting the sensor causes a degradation of the time information, which cannot be recovered to a performance similar to the one achieved by a single channel sensor, even when averaging the ToA of the different channels. In case of the first photon, the optimal CTR for each segmentation is obtained by just using the first averaged channels to compute the timestamp.

For the analogic SiPM, we found that setting the discriminator threshold at the level of the first photon achieves the best performance (fig. 7a,7b,7c , 8a,8b,8c). This has been already observed in experimental measurements [12]. Additionally, for the case

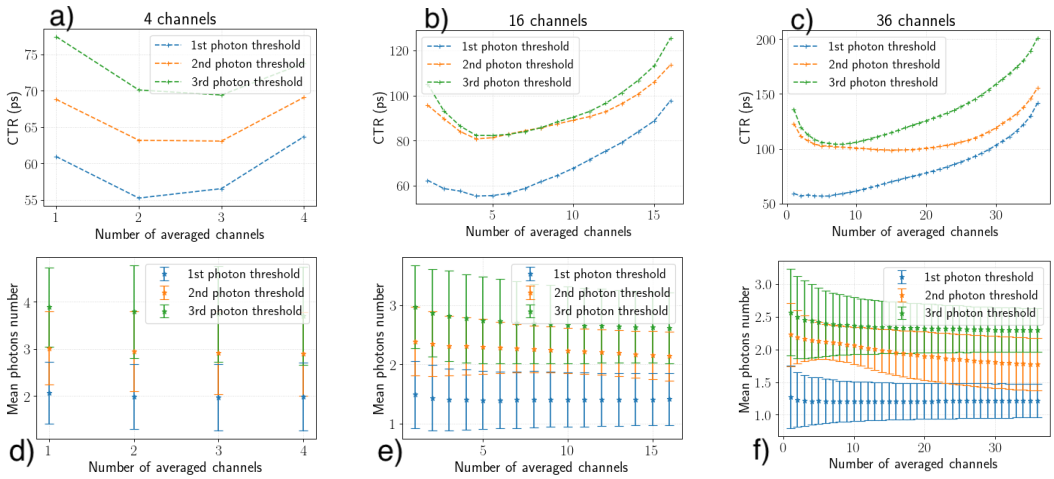


Figure 7: CTR computed for an analog SiPM for 4, 16, 36 channels [a),b) and c) respectively], and the correspondent mean number of photons [d), e), f] for a 5 *mm* LSO crystal.

of the 5 *mm* LSO crystal, we found that independently of the threshold level, it behaves similarly as the digital case when considering the timestamp of the second or a later photon. This is due to the fact that in this case, even when the threshold level is at the first photon level, more than one photon affects to the timestamp acquired (fig. 7d, 7e and 7f). In other words, more than one photon arrives before the stacked SiPM signal crosses the threshold level. Thus, the timestamp generated by the `SSG` function has more dispersion than the ToA of the fastest photon for the digital SiPM. It is worth to note that in the case of a 20 *mm* length crystal with the discriminator threshold at one photon level, the mean number and standard deviation is proximate to one (fig. 8d, 8e, 8f)., which causes a similar behaviour to a digital SiPM of the CTR. This difference in the behaviour of the CTR between the 5 *mm* and 20 *mm* crystal is due to the fact that in the 5 *mm* crystal photons experience less scattering effects, thus having a smaller time spread than in the case of the 20 mm length. Further, it can be deduced from fig. 7 and 8, that for each segmentation, increasing the number of averaged channels, decreases the mean number of photons and its standard deviation.

## 4. Conclusions

In this work, we have studied the timing performance (CTR) for different crystal sizes (5 *mm* and 20 *mm*), type of SiPMs (digital and analog) and sensor segmentations (4, 9, 16, 25 and 36 channels). In order to develop this study, we have created a python package (PyPro) that allow us to compute the CTR for different sensor segmentations and type of sensor.

Simulation results show that for the digital SiPM the best CTR is provided by the fastest channel and fastest photon within the channel, which is the equivalent of having a single channel sensor. Nevertheless, in the case of the fastest photon, there isn't a significant degradation of the optimal CTR when the segmentation increases. For an analog SiPM, the best CTR is provided in each segmentation for the case where the discriminator threshold is set at the lowest level, i.e., at the level of the first photon. This is not always possible to accomplish, thus, in these cases the number of photons

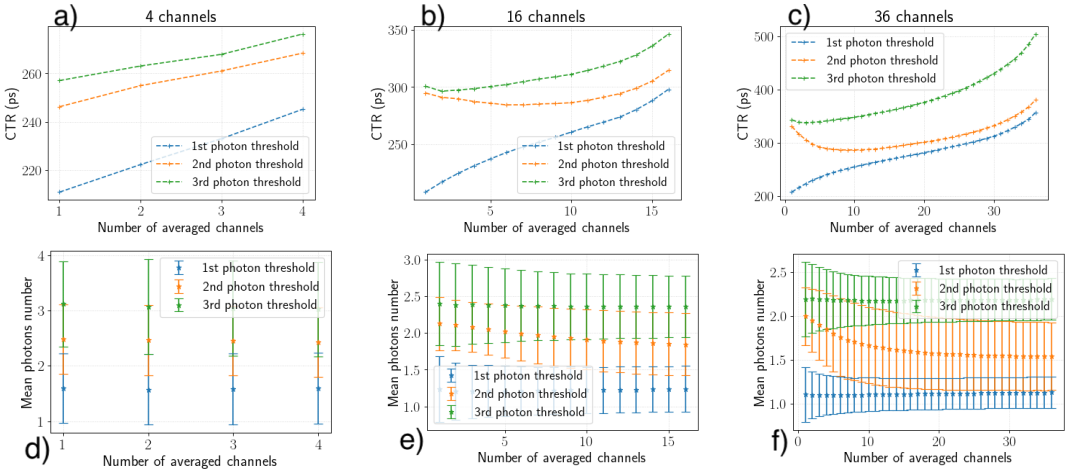


Figure 8: CTR computed for an analog SiPM for 4, 16, 36 channels [a),b) and c) respectively], and the correspondent mean number of photons[d), e), f)] for a 20 *mm* LSO crystal.

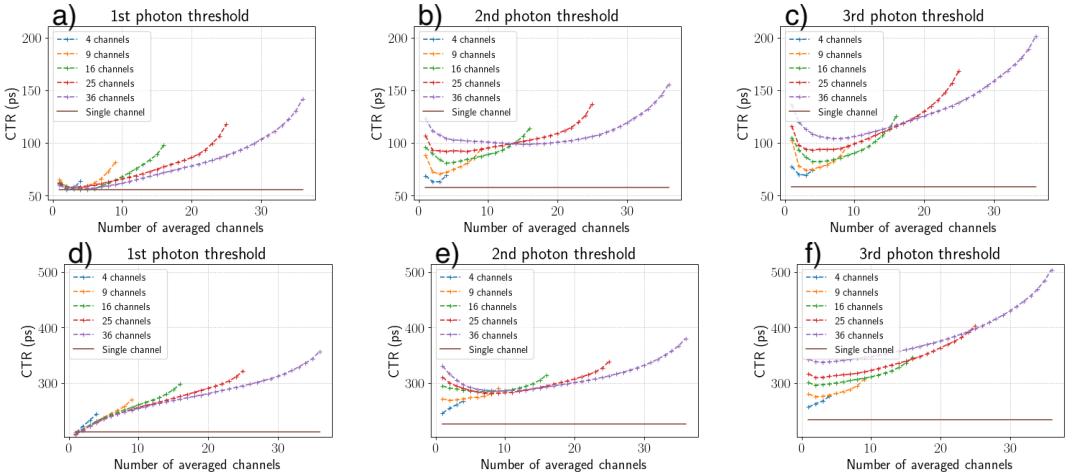


Figure 9: CTR for analog SiPM and discriminator threshold at one, two and three photon level for 5 *mm* [ a),b), c) respectively] and 20 *mm* [ d), e), f)] LSO crystal.

that will contribute to the ToA will be larger and thus more dispersion of the ToA is expected. Thus, if we cannot set the discriminator threshold at the lowest level, results show that the best timing performance is obtained for low segmentations, i.e., for a sensor of 4 and 16 channels. However, even for greater segmentations, the CTR doesn't degrade significantly, since the averaging technique enables to recover part of the information (fig. 9).

It is worth to note that our model only includes the optical part of the PET detector. As we stated in the introduction, in [4], where the electronics were included, authors found an improvement in the timing performance by segmenting the sensor. In fact, they demonstrated that the electronic jitter improved when the sensor was segmented. This is due to the fact that a smaller sensor (larger segmentation) has a lower capacitance, which in turn make the signal faster [13]. Therefore, having in mind that segmenting doesn't degrade the CTR significantly from the optical perspective, and that it reduces the electronic jitter contribution to the time response, segmenting would be expected

to have an increase of timing performance for the full PET module. Additionally, our results could be improved by using the electronic signal that corresponds to each segmentation, since in our model we use the signal associated to a single channel sensor for every segmentation. Another factor that we have not included in our model is the electronic noise. Moreover, we did not introduce the optical noise sources such as the dark count and cross-talks, which could impede the setting of the discriminator threshold at a lower level. The impact of the optical noise in the CTR is not clear and is a future avenue of research. For instance, in a single channel sensor the optical noise events are added to the single signal readout, whereas in a segmented one, not all the channels will be affected by dark counts or crosstalk since the channels are readout individually. Thus, segmenting the sensor in channels and selecting the channels with best time jitter and not affected by the noise sources, could improve the time resolution.

As we have seen, there are several future lines of work to continue with this study, from introducing optical noise, the electronic jitter or the implementation of more complex algorithms to recover the time information lost. In this sense, we find ourselves in an emerging field with a lot of room for improvement. Furthermore, this study has established the groundwork necessary for studying different setups in the next couple of months and has served as an starting point of a doctoral thesis.

## References

[1] S. G. et al., "Time of flight positron emission tomography towards 100ps resolution with l(y)so: An experimental and theoretical analysis," *Journal of Instrumentation*, vol. 8, 7 2013.

[2] P. Lecoq, "Pushing the limits in time-of-flight pet imaging," *IEEE Transactions on Radiation and Plasma Medical Sciences*, vol. 1, pp. 473–485, 11 2017.

[3] J. J. Vaquero and P. Kinahan, "Positron emission tomography: Current challenges and opportunities for technological advances in clinical and preclinical imaging systems.," *Annu Rev Biomed Eng.*, vol. 17, pp. 385–414, 2015.

[4] D. S. et al., "Multimodal simulation of large area silicon photomultipliers for time resolution optimization," *Nuclear Instruments and Methods in Physics Research Section A: Accelerators, Spectrometers, Detectors and Associated Equipment*, vol. 1001, p. 165247, 6 2021.

[5] S. Gundacker and A. Heering, "The silicon photomultiplier: Fundamentals and applications of a modern solid-state photon detector," 9 2020.

[6] S. J. et al., "Gate: a simulation toolkit for pet and spect," *Physics in Medicine and Biology*, vol. 49, pp. 4543–4561, 10 2004.

[7] S. A. et al., "Geant4 - a simulation toolkit," *Nuclear Instruments and Methods in Physics Research, Section A: Accelerators, Spectrometers, Detectors and Associated Equipment*, vol. 506, pp. 250–303, 7 2003.

[8] M. S. et al., "Advanced optical simulation of scintillation detectors in gate v8.0: First implementation of a reflectance model based on measured data," *Physics in Medicine and Biology*, vol. 62, pp. L1–L8, 5 2017.

[9] "Cadence design systems, inc.."

[10] F. Acerbi and S. Gundacker, "Understanding and simulating sipms," *Nuclear Instruments and Methods in Physics Research Section A: Accelerators, Spectrometers, Detectors and Associated Equipment*, vol. 926, pp. 16–35, 2019.

[11] M. Korzhik, G. Tamulaitis, and A. N. Vasil'ev, *Physics of Fast Processes in Scintillators*. Springer International Publishing, 2020.

[12] S. G. et al., "Experimental time resolution limits of modern sipms and tof-pet detectors exploring different scintillators and cherenkov emission," *Physics in Medicine and Biology*, vol. 65, p. 25001, 1 2020.

[13] J. e. a. Fernández-Tenllado, "Optimal design of single-photon sensor front-end electronics for fast-timing applications," in *2019 IEEE Nuclear Science Symposium and Medical Imaging Conference (NSS/MIC)*, pp. 1–5, 2019.